Journal of Sound and Vibration 370 (2016) 1–22

Contents lists available at ScienceDirect

Journal of Sound and Vibration

journal homepage: www.elsevier.com/locate/jsvi

Semi-active vibration control based on unsymmetrical synchronized switch damping: Analysis and experimental validation of control performance

Hongli Ji [a,b,*], Jinhao Qiu [a], Li Cheng [b], Hong Nie [a]

[a] State Key Laboratory of Mechanics and Control of Mechanical Structures, Nanjing University of Aeronautics and Astronautics, Nanjing 210016, China

[b] Department of Mechanical Engineering, Consortium for Sound and Vibration Research, The Hong Kong Polytechnic University, Hung Hom, Kowloon, Hong Kong, China

ARTICLE INFO

Article history:
Received 19 May 2015
Received in revised form
3 December 2015
Accepted 13 January 2016
Handling editor: J. Lam
Available online 19 February 2016

Keywords:
Semi-active vibration control
Piezoelectric elements
Synchronized switch damping
Unsymmetrical circuit

ABSTRACT

In semi-active synchronized switch damping (SSD) approaches for structural vibration control, the damping effect is achieved by properly switching the voltage on the piezoelectric actuators. Unsymmetrical SSD switch circuit has been designed in the previous paper to increase the effective voltage range on the PZT actuator for improvement of the control performance. In this study, analysis and experimental validation of control performance of a synchronized switch damping system based on the unsymmetrical switch circuit are carried out. First the model of an unsymmetrical SSD system is presented and the working principle is introduced. The general expression of the switched voltage on the piezoelectric actuator is derived. Based on its periodicity in steady-state control, the harmonic components of the actuator voltage are derived using Fourier series expansion. Next, the displacement response of the system is derived under combined actions of the excitation and switched voltage. Finally, a setup of a flexible beam with unsymmetrical switch circuit is used to demonstrate the control performance under different voltage sources and to verify the theoretical results. The results show that the control performance mainly depends on the voltage range on the PZT. A higher effective voltage range can be generated in unsymmetrical SSDV than in symmetrical SSDV and better control performance can be achieved at the same negative actuator voltage. The unsymmetrical SSDV makes better utilization of the actuator capability.

1. Introduction

With the rapid development of the aerospace industry, the control of aircraft structural vibration becomes increasingly important. Semi-active switched-voltage control using piezoelectric actuators has been an active area of research since it was first proposed by Richard et al. in 1998 because of its simple implementation in practical systems [1,2]. In the semi-active switched-voltage control the voltage on the piezoelectric element is switched at the strain extrema or displacement extrema of vibration and therefore these methods are called Synchronized Switch Damping (SSD) approaches. Since no

* Corresponding author.
E-mail address: jihongli@nuaa.edu.cn (H. Ji).

http://dx.doi.org/10.1016/j.jsv.2016.01.033
0022-460X/

proportional power amplifiers and high-performance digital signal processing units are required, these systems are easy to implement for practical applications. They also consume less energy than the active bang–bang control [3,4], because the energy applied to the piezoelectric actuator is delivered by an external source in bang–bang control. Due to fast inversion of voltage on the piezoelectric actuators by a resonant shunt circuit, the power consumed by a semi-active control system is usually very low [5,6]. Several variances of the SSD method, including Synchronized Switch Damping on Inductor (SSDI) [7], Synchronized Switch Damping on Voltage source (SSDV) [8,9], adaptive SSDV [10–12], and SSDNC (SSD based on negative capacitor) have been developed in the past ten years [13–15]. Since switching phase and switching frequency are critical factors to damping performance in SSD method, their influence on converted energy has been investigated [16]. Many switching control algorithms have been developed to maximize the energy dissipated in each cycle of vibration [17–19].

Although a multitude of outstanding works has been made in SSD control [20,21], the generated voltage on the PZT is symmetrical in the original SSD method. But due to the inherent properties of piezoelectric materials, the applicable bipolar voltage of a piezoelectric actuator is unsymmetrical. That is, the voltage applicable in the positive direction (poled direction) is much higher than that in the negative direction because the applicable positive voltage depends on the electrical breakdown voltage of the piezoelectric material, but the applicable negative voltage depends on its depoling voltage. The typical electric field applicable in the positive direction is higher than 2000 V/mm, but that in the negative direction is only about 500 V/mm. As an example of applicable voltage on an actuator, the working voltage range of MFC actuators is from -500 V to 1500 V. If symmetrical switching circuit is used, the voltage range will be from -500 V to 500 V, so that half of the actuator capability will be wasted.

To solve this problem, an unsymmetrical switch circuit was designed for high-voltage semi-active control method based on SSDV by Ji et al. [22]. A bypass capacitor and an additional switch are used to realize unsymmetrical bipolar voltage. Experiments were carried out to verify the designed circuit. Experimental results show that the designed circuit can generate a high unsymmetrical voltage on the piezoelectric actuators. In this paper, further research works on theoretical formulation and control experiments of unsymmetrical SSDV are conducted based on the work in the previous paper.

In this study, analysis and experimental validation of the control performance using the unsymmetrical circuit are carried out. The control performance of symmetrical SSD control was systematically investigated by Ji et al. based on the concept of energy conversion [22]. In this paper, the time-domain approach is used. In Section 2, the model of an unsymmetrical SSD system is presented and the working principle is introduced. The general expression of the actuator voltage on the piezoelectric actuator is derived. In Section 3, the structural response with unsymmetrical SSD control is derived. In the analysis of system response, the influence of leakage on the switched voltage is taken into consideration, but the transient process of leakage is neglected. In Section 4, a setup of a flexible beam with unsymmetrical SSD is used to demonstrate the control performance of unsymmetrical SSD control. The results show that the control performance mainly depends on the effective range of switched voltage on the PZT. Finally, some concluding remarks are given in Section 5.

2. Modeling of structures using unsymmetrical SSD control

2.1. Electromechanical model of a vibration system

The electromechanical model of a vibration system is the basis for analysis and design of SSD control systems. Modeling of the structural system with SSD control has been discussed in former studies [23,24]. A continuous structure can also be modeled as a multi-degree-of-freedom system after modal truncation [25]. In this study, the typical electromechanical model based on a spring-mass system with only one degree of freedom, as shown in Fig. 1, is used. This model gives a good description of the vibrating behavior of a structure near a resonance [23]. The governing equation of the electromechanical model is given by

$$M\ddot{u}+C\dot{u}+K_E u=\sum F_i \tag{1}$$

where M represents the equivalent rigid mass, C is the inherent structural damping coefficient, K_E is the equivalent stiffness of

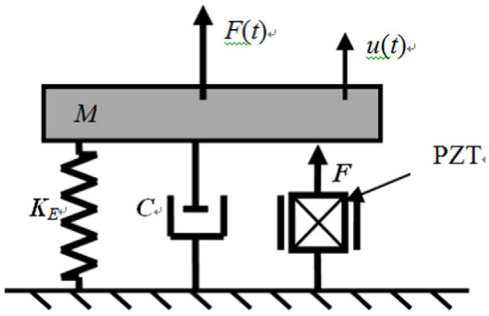

Fig. 1. A single SDOF with a piezoelectric transducer.

the structural system, which can be expressed as

$$K_E = K_s + K^{sc} \tag{2}$$

where K_s is the stiffness of the host structure and the K^{sc} is the stiffness of the piezoelectric transducer in short circuit. u is the rigid mass displacement and $\sum F_i$ represents the sum of other forces applied to the equivalent rigid mass, comprising forces applied by piezoelectric elements. Piezoelectric elements bonded on the considered structure ensure the electromechanical coupling, which is described by

$$F_p = -\alpha V_a \tag{3}$$

$$I = \alpha \dot{u} - C_p \dot{V}_a \tag{4}$$

where F_p is the electrically dependent part of the force generated by piezoelectric elements on the structure, V_a is the voltage on the piezoelectric elements, C_p is the blocked capacitance of piezoelectric elements, α is the force factor, and I is the outgoing current from piezoelectric elements. M, C_p, α and K_E can be deduced from piezoelectric elements and structure characteristics and geometry.

Finally, $\sum F_i$ applied to the rigid equivalent mass comprises F_p and an external excitation force F_e. Thus, the differential equation governing the mass motion can be written as

$$M\ddot{u} + C\dot{u} + K_E u = F_e - \alpha V_a \tag{5}$$

In the following analysis, it is assumed that the excitation and response have the following form:

$$F_e = F_M \sin \omega_e t, u(t) = -u_M \cos(\omega_e t - \varphi_u). \tag{6}$$

where F_M is the amplitude of the excitation force, ω_e is the angular frequency of excitation, which may not be equal to the angular natural frequency of the system ω_n. $\varphi_u + \pi/2$ is the phase delay of the displacement with respect to the exciting force.

After Eq. (6) is substituted into Eq. (5), the amplitude and phase of displacement without control can be obtained. In harmonic motion the phases of velocity and acceleration lead the displacement by 90° and 180°, respectively. When there is no control, the amplitude and phase of vibration can be expressed in the following form:

$$\begin{cases} u_M = \dfrac{F_M}{\sqrt{(K_E - M\omega_e^2)^2 + (C\omega_e)^2}} = \dfrac{F_M/K_E}{\sqrt{\left(1 - \left(\frac{\omega_e}{\omega_n}\right)^2\right)^2 + \left(2\left(\frac{\omega_e}{\omega_n}\right)\xi\right)^2}} \\ \tan \varphi_u = -\dfrac{K_E - M\omega_e^2}{C\omega_e} = -\dfrac{1 - (\omega_e/\omega_n)^2}{2\xi} \end{cases} \tag{7}$$

where $\omega_n = \sqrt{K_E/M}$ is the natural frequency of undamped oscillation, and $\zeta = C/2M\omega_n$ is the damping ratio.

2.2. Principle of unsymmetrical SSD method and the actuator voltage

2.2.1. Principle of unsymmetrical SSD method

An unsymmetrical SSD switch circuit to increase the effective actuator voltage range on the PZT has been designed by Ji et al. [22]. The schematic diagram of the unsymmetrical SSDV control system is shown in Fig. 2(a). It is different from the classical SSDV in that a unidirectional bypass capacitor C_b and a switch SW3 are connected in parallel to the piezoelectric actuator, which is used to realize the unsymmetrical voltage inversion on the piezoelectric element. In order to obtain unsymmetrical actuator voltage, the switching logic is used to control the three switchers: SW1 is closed at every maximum

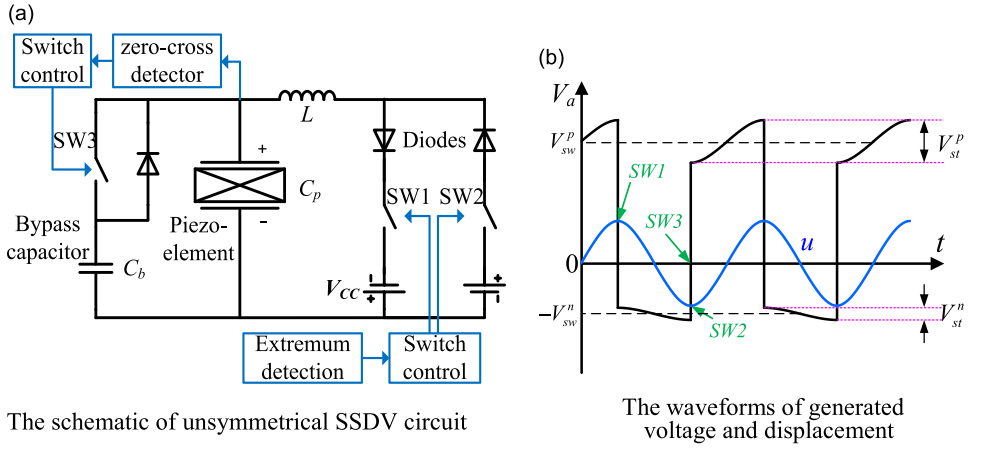

Fig. 2. Principle of unsymmetrical SSDV. (a) The schematic of unsymmetrical SSDV circuit. (b) The waveforms of generated voltage and displacement.

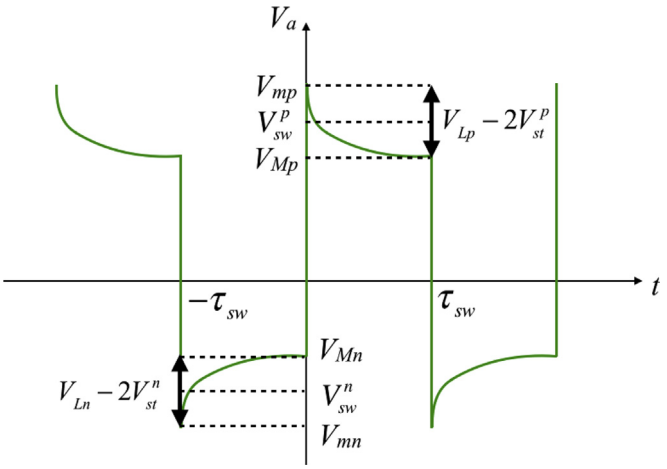

Fig. 3. The variation of actuator voltage due to leakage.

of displacement and is kept closed for half a period of electrical oscillator; SW2 is closed at every minimum of displacement and is kept closed for half a period of electrical oscillator; SW3 is closed at the same time with SW2, but it is kept closed until the voltage on the piezoelectric actuator equals 0. The unsymmetrical switched voltage is schematically shown in Fig. 2(b).

2.2.2. The generated voltage on the actuator

In the early studies of SSDV control, the actuator voltage, $V_a(t)$, was usually decomposed into two components: V_{st}, the voltage induced by mechanical strain, and V_{sw}, the voltage due to switching action [10,11]. The actuator voltage has a waveform as shown in Fig. 2(b). However, the former studies indicated that the leakage of the switch circuit must be taken into consideration when the switching frequency is as low as a few Hertz [22]. Hence, the actuator voltage can be expressed in the following form:

$$V_a(t) = V_{st}(t) + V_{sw}(t) + V_L(t) \tag{8}$$

where $V_L(t)$ is the voltage due to leakage.

The schematic waveform of actuator voltage is shown in Fig. 3 when the leakage is not negligible under the assumption that $\varphi_u = 0$ in the displacement response. Because the leakage $V_L(t)$ has a greater contribution than the voltage induced by mechanical strain, the actuator voltage decreases when the switch circuit is in the open-circuit state [22].

In the following discussions, it is assumed that the actuator voltage is switched at the displacement extrema. It means that voltage is switched twice in each vibration cycle and the switching frequency is twice that of the vibration to be controlled.

Based on the displacement in Eq. (6), the switching points are

$$t_k = kT_{sw} + \tau_u (k = 0, \pm 1, \pm 2\cdots). \tag{9}$$

where T_{sw}, defined as the switching period $T_{sw} = \pi/\omega_e$, is the time between two neighboring switching points and $\tau_u = \varphi_u/\omega_e$. If the frequency of excitation is the same as the resonance frequency, the phase angle, φ_u, in Eq. (6) is 0. In that case the voltage shown in Fig. 3 is obtained.

Since the period of the switch circuit is much shorter than the period of mechanical vibration, it is also assumed that voltage inversion is completed instantly at the switching points. Under this assumption, the actuator voltage, $V_a(t)$, is a piece-wise smooth function. It jumps from $-V_{Mn}$ to V_{mp} at $t_{2k} = 2kT_{sw} + \tau_u$ and from V_{Mp} to $-V_{mn}$ at $t_{2k+1} = (2k+1)T_{sw} + \tau_u$. It varies smoothly from V_{mp} to V_{Mp} between t_{2k}^+ to t_{2k+1}^- and from $-V_{mn}$ to $-V_{Mp}$ between t_{2k-1}^+ to t_{2k}^-. The superscripts, "+" and "−", mean "immediately after" and "immediately before", in the same way as they are used in calculus. The switched voltage, V_{sw}, is constant between two switching points, but V_{st} and $V_L(t)$ vary with time. The magnitudes of positive and negative switched voltages are defined as follows

$$V_{sw}^p = (V_{mp} + V_{Mp})/2, \quad V_{sw}^n = (V_{mn} + V_{Mn})/2. \tag{10}$$

2.2.3. The strain-induced voltage

According to the configuration of the circuit, the voltage induced by strain can be expressed by

$$V_{st}(t) = \begin{cases} V_{st}^p(t) = \dfrac{\alpha}{C_p} u(t), & \text{for } u^a \geq 0) \\ V_{st}^n(t) = \dfrac{\alpha}{C_p + C_b} u(t), & \text{for } u^a < 0) \end{cases} \tag{11}$$

where C_b is a unidirectional bypass capacitor as shown in Fig. 2(a). Eq. (11) means that $V_{st}(t)=V_{st}^{p}(t)$ when the displacement varies from $-u_M$ to u_M, and $V_{st}(t)=V_{st}^{n}(t)$ when the displacement varies from u_M to $-u_M$. Obviously, the converted energy due to $V_{st}(t)$ is zero.

The displacement expression in Eq. (6) indicates that $\dot{u}>0$ when $2kT_{sw}+\tau_u \le t<(2k+1)T_{sw}+\tau_u$ and $\dot{u}<0$ when $(2k-1)T_{sw}+\tau_u \le t<2kT_{sw}+\tau_u$ $(k=0,\pm1,\pm2,\cdots)$. Obviously, there exist

$$\begin{cases} V_{st}(t_{2k}^{+})=-\dfrac{\alpha}{C_p}u_M, & V_{st}(t_{2k+1}^{-})=\dfrac{\alpha}{C_p}u_M \\ V_{st}(t_{2k-1}^{+})=\dfrac{\alpha}{C_p+C_b}u_M, & V_{st}(t_{2k}^{-})=-\dfrac{\alpha}{C_p+C_b}u_M \end{cases}. \tag{12}$$

2.2.4. The switched voltage

The switched voltage, $V_{sw}(t)$, in unsymmetrical SSD control can be expressed in the following form:

$$V_{sw}(t)=\begin{cases} V_{sw}^{p}, & \text{for } u^{a}\ge 0) \\ -V_{sw}^{n}, & \text{for } u^{a}<0) \end{cases} \tag{13}$$

where V_{sw}^{p} and V_{sw}^{n} are magnitudes of the positive and negative voltages, respectively.

As shown in the former study [22], and in unsymmetrical SSD control can be expressed in the following form:

$$\begin{cases} V_{sw}^{p}=a^{p}\dfrac{\alpha u_M}{C_p}+b_p^{p}V_{cc}^{p}+b_n^{p}V_{cc}^{n}-c_p^{p}V_{Lp}-c_n^{p}V_{Ln} \\ V_{sw}^{n}=a^{n}\dfrac{\alpha u_M}{C_p}+b_p^{n}V_{cc}^{p}+b_n^{n}V_{cc}^{n}-c_p^{n}V_{Lp}-c_n^{n}V_{Ln} \end{cases} \tag{14}$$

where V_{cc}^{p} and V_{cc}^{n}, both take positive values and are the positive and negative voltage sources, and V_{Lp} and V_{Ln}, both take positive values too and are the voltage drops induced by leakage between switch points when the actuator voltage is positive and negative, respectively. The coefficients a^p, a^n, b_p^p, b_p^n, b_n^p, b_n^n, c_p^p, c_p^n, c_n^p, and c_n^n can easily be obtained from the equations in Ref. [22]. Eq. (14) indicates that the switched voltage depends on the amplitude of vibration, the output of positive and negative voltage sources, and the voltage drops due to leakage.

As shown in Eq. (13), in the steady-state control using unsymmetrical SSD method, the switched voltage on the piezoelectric actuator, V_{sw}, is a biased rectangular waveform, with its positive voltage equal to , and its negative voltage equal to $-V_{sw}^{n}$. The bias voltage, $\overline{V}_{sw}$, and the amplitude, $\hat{V}_{sw}$, of V_{sw} can be expressed by

$$\begin{cases} \overline{V}_{sw}=\dfrac{1}{2}(V_{sw}^{p}-V_{sw}^{n}) \\ \hat{V}_{sw}=\dfrac{1}{2}(V_{sw}^{p}+V_{sw}^{n}) \end{cases} \tag{15}$$

The switched voltage V_{sw} can be expressed as

$$V_{sw}(t)=\overline{V}_{sw}+\tilde{V}_{sw}(t)=\overline{V}_{sw}+\hat{V}_{sw}S_{\tau_{sw}}(t) \tag{16}$$

where $S_{\tau_{sw}}(t)$ is a switch function defined by

$$S_{\tau_{sw}}(t)=\begin{cases} -1 & t_{2k-1}\le t<t_{2k} \\ +1 & t_{2k}\le t<t_{2k+1} \end{cases}(k=0,\pm1,\pm2\cdots) \tag{17}$$

In Eq. (16), $\tilde{V}_{sw}(t)=\hat{V}_{sw}S_{\tau_{sw}}(t)$ is symmetrical rectangular waveform. The angular switching frequency is defined as

$$\omega_{sw}=\frac{2\pi}{T_{sw}}. \tag{18}$$

2.2.5. The voltage due to leakage

Similarly, the variation of voltage due to leakage can be expressed in the following form:

$$V_L(t)=\begin{cases} V_L^{p}(t), & \text{for } V_a\ge 0 \\ V_L^{n}(t), & \text{for } V_a<0 \end{cases} \tag{19}$$

According to the results in Ref. [22], the variation of voltage due to leakage, $V_L^p(t)$ and $V_L^n(t)$ in Eq. (19), can be expressed as

$$\begin{cases} V_L^{p}(t)=\frac{1}{2}V_{Lp}-(V_{sw}^{p}+\frac{1}{2}V_{Lp})\left[\overline{b}(t-t_k)+\overline{c}(1-e^{-d(t-t_k)})+\overline{f}(1-e^{-g(t-t_k)})\right](t_{2k}\le t<t_{2k+1},\text{where}k=0,\pm1,\pm2\cdots) \\ V_L^{n}(t)=-\frac{1}{2}V_{Ln}+(V_{sw}^{n}+\frac{1}{2}V_{Ln})\left[\overline{b}'(t-t_k)+\overline{c}'(1-e^{-d(t-t_k)})+\overline{f}'(1-e^{-g(t-t_k)})\right](t_{2k-1}\le t<t_{2k},\text{where}k=0,\pm1,\pm2\cdots) \end{cases} \tag{20}$$

where $\overline{b},\overline{b}',\overline{c},\overline{c}',\overline{f},\overline{f}'$ are coefficients, which can easily be obtained from the equation in Ref. [22]. According to the definitions

of and , and the definitions of V_L^p, V_L^n, V_{Lp} and V_{Ln}, there exist

$$\begin{cases} V_L(t_{2k}^+) = V_L^p(t_{2k}^+) = \dfrac{1}{2}V_{Lp}, & V_L(t_{2k+1}^-) = V_L^p(t_{2k+1}^-) = -\dfrac{1}{2}V_{Lp} \\ V_L(t_{2k-1}^+) = V_L^n(t_{2k-1}^+) = -\dfrac{1}{2}V_{Ln}, & V_L(t_{2k}^-) = V_L^n(t_{2k}^-) = \dfrac{1}{2}V_{Ln} \end{cases}. \tag{21}$$

The transient leakage voltages, $V_L^p(t)$ and $V_L^n(t)$ in Eq. (20), can be written as

$$\begin{cases} V_L^p(t) = \left[\dfrac{1}{2} - L^p(t-t_{2k})\right]V_{Lp} & (t_{2k} \le t < t_{2k+1}, \text{where} k = 0, \pm 1, \pm 2\cdots) \\ V_L^n(t) = -\left[\dfrac{1}{2} - L^n(t-t_k)\right]V_{Ln} & (t_{2k-1} \le t < t_{2k}, \text{where} k = 0, \pm 1, \pm 2\cdots) \end{cases} \tag{22}$$

where

$$\begin{cases} L^p(t) = \dfrac{\bar{b}t + \bar{c}(1-e^{-dt}) + \bar{f}(1-e^{-gt})}{\bar{b}T_{sw} + \bar{c} + \bar{f}} \\ L^n(t) = \dfrac{\bar{b}'t + \bar{c}'(1-e^{-dt}) + \bar{f}'(1-e^{-gt})}{\bar{b}'T_{sw} + \bar{c}' + \bar{f}'} \end{cases} \tag{23}$$

for $0 < t < T_{sw}$. The above expressions have been simplified with the assumption that $dT_{\rm sw}, gT_{\rm sw}$, $d'T_{\rm sw}, g'T_{\rm sw}$ are large enough so that $e^{-dT_{\rm sw}} = e^{-gT_{\rm sw}} = e^{-d'T_{\rm sw}} = e^{-g'T_{\rm sw}} = 0$. In the experimental conditions of this study, these assumptions are satisfied.

Obviously, both $L^p(t)$ and $L^n(t)$ are monotone increasing functions, satisfying the conditions

$$L^p(0) = L^n(0) = 0, \quad L^p(T_{\rm sw}) = L^n(T_{\rm sw}) = 1. \tag{24}$$

2.2.6. The actuator voltage

Summarizing the above results, the actuator voltage can be expressed in the following form:

$$V_a(t) = \begin{cases} V_a^p, & \text{for } \dot{u} > 0 \ (V_a \ge 0) \\ V_a^n, & \text{for } \dot{u} < 0 \ (V_a < 0) \end{cases} \tag{25}$$

where V_a^p and V_a^n are given by

$$\begin{cases} V_a^p(t) = V_{\rm st}^p(t) + V_{\rm sw}^p(t) + V_L^p(t) \\ V_a^n(t) = V_{\rm st}^n(t) + V_{\rm sw}^n(t) + V_L^n(t) \end{cases}. \tag{26}$$

Obviously, there exist

$$\begin{cases} V_a(t_{2k}^+) = V_{mp} = V_{\rm sw}^p - \dfrac{\alpha}{C_p}u_M + \dfrac{V_{Lp}}{2}, \\ V_a(t_{2k+1}^-) = V_{Mp} = V_{\rm sw}^p + \dfrac{\alpha}{C_p}u_M - \dfrac{V_{Lp}}{2}, \\ V_a(t_{2k-1}^+) = -V_{mn} = -V_{sw}^n + \dfrac{\alpha}{C_p + C_b}u_M - \dfrac{V_{Ln}}{2}, \\ V_a(t_{2k}^-) = -V_{Mn} = -V_{\rm sw}^n - \dfrac{\alpha}{C_p + C_b}u_M + \dfrac{V_{Ln}}{2}. \end{cases} \tag{27}$$

2.3. The Fourier series expansion of actuator voltage

Although the actuator voltage is unsymmetrical, it is periodic. Its frequency is the same as the harmonic vibration used for switch control. It is also half of the switching frequency because the switch is closed twice in each cycle of mechanical vibration. In order to investigate its influence on the mechanical vibration, the actuator voltage is expressed in Fourier series.

With the assumption of excitation and response in Eq. (6), the switch points are given in Eq. (9). Because $t = 0$ is not a switching point, the Fourier expansion of the actuator voltage will be very complicated. For convenience, it is first assumed that the initial phase of displacement, φ_u, is zero and the period of actuator voltage used for Fourier expansion is $-T_{\rm sw} \le t < T_{\rm sw}$. If the Fourier expansion of $V_a(t)$ is expressed by $\mathcal{F}\{V_a(t)\}$, then there exists

$$V_a(t) = \mathcal{F}\{V_a(t)\} = \frac{a_0^a}{2} + \sum_{k=1}^{\infty}\left(a_k^a \cos k\frac{\omega_{\rm sw}}{2}t + b_k^a \sin k\frac{\omega_{\rm sw}}{2}t\right). \tag{28}$$

Obviously, the Fourier expansion of the actuator voltage is the sum of the Fourier expansion of all the components. That is,

$$\mathcal{F}\{V_a(t)\}=\mathcal{F}\{V_{st}(t)\}+\mathcal{F}\{V_{sw}(t)\}+\mathcal{F}\{V_L(t)\}. \tag{29}$$

The derivations of the Fourier coefficients of every component are shown in Appendix A. The Fourier expansion of $V_a(t)$ can be expressed in the following form:

$$V_a(t)=\frac{a_0}{2}+\sum_{k=1}^{\infty}(a_k\ \cos\ k\omega_e t+b_k\ \sin\ k\omega_e t). \tag{30}$$

where

$$\begin{cases} a_0=a_0^{st}+a_0^{sw}+a_0^{L} \\ a_k=a_k^{st}+a_k^{sw}+a_k^{L} \\ b_k=b_k^{st}+b_k^{sw}+b_k^{L} \end{cases}, \tag{31}$$

The constants on the right-hand side of each expression in Eq. (31) are derived in Appendix A. Eq. (30) shows that due to the switching action, the actuator voltage contains the high-order harmonic components. That is why high-order components of mechanical vibration are induced in semi-active control. Moreover, due to unsymmetrical switching, the actuator voltage also contains a DC component, denoted by $a_0/2$.

In Eq. (30), the initial phase φ_u has been assumed to be 0. If φ_u is not 0, the actuator voltage $V_a(t)$ is shifted by τ_u in time domain. Hence, the Fourier expansion of $V_a(t)$ with nonzero φ_u can be expressed in the following form:

$$V_a(t)=\frac{a_0}{2}+\sum_{k=1}^{\infty}\left[a_k\ \cos\ k(\omega_e t-\varphi_u)+b_k\ \sin\ k(\omega_e t-\varphi_u)\right]. \tag{32}$$

3. Displacement response in unsymmetrical SSD control

According to the equation of motion Eq. (5), the displacement response with SSDV control is the solution of Eq. (5) with both the nonhomogeneous terms F_e and $-\alpha V_a$ on the right-hand side. Due to its linearity, the solution of Eq. (5) obeys the superposition principle. Hence, we only need to consider the response of system under the influence of different components separately. The total response can be expressed in the following form:

$$u(t)=u_0+\sum_{k=1}^{\infty}u_{kM}\ \cos\left(k\omega_e t-\varphi_k\right). \tag{33}$$

where u_0 is the static displacement generated by the DC voltage component in Eq. (30) and each high-order harmonic component in Eq. (33) is generated by the corresponding voltage component with the same frequency. The fundamental component is influenced by both the excitation force and the fundamental harmonic in Eq. (32).

According to Eq. (6), $\varphi_1=\pi+\varphi_u$; when the vibration is excited at the resonance frequency, $\varphi_u=0$ and $\varphi_1=\pi$.

3.1. Output of voltage source and switched voltage

As shown in Eq. (14), the switched voltage depends on both the output of the voltage sources and the leakage. For convenience, it is assumed that the outputs of the positive voltage source and the negative voltage source, V_{cc}^p and V_{cc}^n, are the same and proportional to the displacement amplitude, u_M, that is,

$$V_{cc}^p=V_{cc}^n=\frac{\alpha}{C_p}\beta u_M. \tag{34}$$

where β is the proportional coefficient.

According to Eqs. (14) and (15), the amplitude of switched voltage, $\hat{V}_{\mathrm{sw}}$, can be expressed as,

$$\begin{cases} V_{\mathrm{sw}}^p=\left(a^p+\beta b_p^p+\beta b_n^p\right)\frac{\alpha u_M}{C_p}-c_p^pV_{Lp}-c_n^pV_{Ln} \\ V_{\mathrm{sw}}^n=\left(a^n+\beta b_p^n+\beta b_n^n\right)\frac{\alpha u_M}{C_p}-c_p^nV_{Lp}-c_n^nV_{Ln} \end{cases} \tag{35}$$

$$\begin{cases} \overline{V}_{\mathrm{sw}}=\frac{1}{2}\left[(a^p-a^n)\frac{\alpha u_M}{C_p}+\left(b_p^p+b_n^p-b_p^n-b_n^n\right)\frac{\alpha\beta u_M}{C_p}\right]-\frac{1}{2}\left[\left(c_p^p-c_p^n\right)V_{Lp}+(c_n^p-c_n^n)V_{Ln}\right] \\ \hat{V}_{\mathrm{sw}}=\frac{1}{2}\left[(a^p+a^n)\frac{\alpha u_M}{C_p}+\left(b_p^p+b_n^p+b_p^n+b_n^n\right)\frac{\alpha\beta u_M}{C_p}\right]-\frac{1}{2}\left[\left(c_p^p+c_p^n\right)V_{Lp}+(c_n^p+c_n^n)V_{Ln}\right]. \end{cases} \tag{36}$$

In the above equations, $\alpha u_M(a^p+a^n)/C_p$ is contributed by the voltage generated by mechanical strain. In SSDV control, it is usually much smaller than the other terms. The drop of voltage due to leakage depends on the output of voltage source,

V_{cc}^p and V_{cc}^n. The results of the former study indicated that leakage becomes more intense as the switched voltage increases based on high V_{cc}^p and V_{cc}^n. Hence, when $V_{cc}^p = V_{cc}^n$, we simply express the V_{Lp} and V_{Ln} in the following form:

$$\begin{cases} V_{Lp} = AV_{cc}^p = A\frac{\alpha}{C_p}\beta u_M \\ V_{Ln} = BV_{cc}^p = B\frac{\alpha}{C_p}\beta u_M \end{cases}, \tag{37}$$

where the coefficients A and B are not constants because their relationships are not linear [22]. They are functions V_{cc}^p, C_p, C_b and other parameters of the circuit. Using Eqs. (36) and (37), and neglecting the voltage due to strain, the magnitude of switched voltage is expressed as

$$\hat{V}_{sw} = \frac{1}{2}\left[\left(b_p^p + b_n^p + b_p^n + b_n^n\right) - A\left(c_p^p + c_p^n\right) - B\left(c_n^p + c_n^n\right)\right]\frac{\alpha\beta u_M}{C_p} = H\frac{\alpha\beta u_M}{C_p} \tag{38}$$

where

$$H = \frac{1}{2}\left[\left(b_p^p + b_n^p + b_p^n + b_n^n\right) - A\left(c_p^p + c_p^n\right) - B\left(c_n^p + c_n^n\right)\right]. \tag{39}$$

3.2. The static displacement due to DC voltage component

According to Eqs. (30) and (31), the DC component, $a_0/2$, can be expressed in the following:

$$\frac{a_0}{2} = \overline{V}_{\mathrm{sw}} + a_0^L, \tag{40}$$

In the static force of $a_0/2$, the solution of Eq. (5) can be expressed as

$$u_0 = -\alpha\left(\overline{V}_{\mathrm{sw}} + a_0^L\right)/K^E \tag{41}$$

This is the static displacement produced in unsymmetrical SSDV control. Usually a_0^L is much smaller than $\overline{V}_{\mathrm{sw}}$, and its influence is negligible.

3.3. Damping effect without considering transient leakage

The circuit leakage influences the damping effect in two aspects: it reduces the switched voltage as shown in Eq. (14) in one aspect, and it generates a transient component $V_L(t)$ in the other aspect. In this section, the influence of $V_L(t)$ on damping effect is neglected. On the other hand, since resonant vibration is much stronger than non-resonant vibration, resonant vibration is considered first.

When the system is excited at the resonance frequency of ith mode, the displacement of this mode is dominant in the system response. The response is simultaneously generated by the excitation force F_e and the fundamental harmonic in the actuator voltage, $a_1 \cos \omega_e t + b_1 \sin \omega_e t$. The equation of motion is written as

$$M_i\ddot{u}_i + C_i\dot{u}_i + K_{Ei}u_i = F_e - \alpha_i(a_1 \cos \omega_e t + b_1 \sin \omega_e t) \tag{42}$$

A subscript i is added to Eq. (5) to distinguish the modal number.

According to Eq. (31), neglecting the transient component of leakage, there exist

$$\begin{cases} a_1 = a_1^{st} + a_1^{sw} = -\frac{\alpha_i u_{iM}}{2}\frac{2C_p + C_b}{C_p(C_p + C_b)} \\ b_1 = b_1^{st} + b_1^{sw} = \frac{4}{\pi}\hat{V}_{\mathrm{sw}} \end{cases}, \tag{43}$$

Obviously, the cosine term on the right side of Eq. (42) has the opposite phase as u_i and its effect increases the stiffness of the system. Hence, Eq. (42) can be expressed in the following form:

$$M_i\ddot{u}_i + C_i\dot{u}_i + K_{Di}u_i = F_e - \frac{4\alpha_i}{\pi}\hat{V}_{\mathrm{sw}} \sin \omega_e t \tag{44}$$

when excited at the resonance frequency, the amplitude of the fundamental harmonic is

$$u_{iM} = \frac{F_M}{\omega_e C_i + \frac{4}{\pi}\cdot\frac{\alpha_i^2}{C_p}\cdot\beta H} \tag{45}$$

The attenuation is defined as:

$$A_{\mathrm{ASSDV}} = 20\log\left(\frac{u_{iM}}{\overline{u}_{iM}}\right) = -20\log\left(1 + \frac{4}{\pi}\cdot\beta H\cdot K_{sii}Q_{mi}\right) \tag{46}$$

where $\overline{u}_{iM}$ is the amplitude without control, and K_{sii} and Q_{mi} are structural coupling factor and mechanical quality factor of

the ith mode, respectively. They are defined as follows

$$K_{sii}=\frac{{\alpha_i}^2}{K_{Di}C_p},\qquad Q_{mi}=\frac{2\sqrt{K_{Di}M_i}}{C_i}. \tag{47}$$

When vibration is not excited at the resonance frequency, the amplitude and phase angle can be obtained by solving the equation of motion in Eq. (5). The results are

$$\begin{cases} u_{iM}=\dfrac{F_M}{\sqrt{\left(K_{Di}-\omega_e^2M_i\right)^2+\left(\omega_eC_i+\frac{4}{\pi}\cdot\frac{\alpha_i^2}{C_p}\cdot\beta H\right)^2}}=\dfrac{F_M/K_{Di}}{\sqrt{\left(1-\left(\frac{\omega_e}{\omega_{ni}}\right)^2\right)^2+\left[2\left(\frac{\omega_e}{\omega_{ni}}\right)\zeta_i+\frac{4}{\pi}\cdot K_{sii}\beta H\right]^2}} \\ \tan\,\varphi=-\dfrac{1-\left(\frac{\omega_e}{\omega_{ni}}\right)^2}{2\left(\frac{\omega_e}{\omega_{ni}}\right)\zeta_i+\frac{4}{\pi}\cdot K_{sii}\beta H} \end{cases} \tag{48}$$

where ω_{ni} is the natural frequency of the ith mode. When the system is excited at non-resonance frequency, the attenuation is

$$A_{\mathrm{ASSDV}}=20\log\left(\frac{u_{iM}}{\bar{u}_{iM}}\right)=20\log\frac{\sqrt{\left(1-\left(\frac{\omega_e}{\omega_{ni}}\right)^2\right)^2+\left[2\left(\frac{\omega_e}{\omega_{ni}}\right)\zeta_i\right]^2}}{\sqrt{\left[1-\left(\frac{\omega_e}{\omega_{ni}}\right)^2\right]^2+\left[2\left(\frac{\omega_e}{\omega_{ni}}\right)\zeta_i+\frac{4}{\pi}\cdot K_{sii}\beta H\right]^2}} \tag{49}$$

3.4. Influence of switched voltage on other modes

As shown in Eq. (30), high-order harmonic components are generated in the actuator voltage by the switching process. These high-order harmonic components of actuator voltage will produce actuator forces, which in turn will excite high-order harmonic components of system vibration. A high-order harmonic vibration may not be negligible when the frequency of excitation is not far from the natural frequency of a high-order mode. In this section, the influence of switched voltage on other modes is briefly discussed.

Since the high-order harmonic components of switched voltage are much larger than the corresponding components due to strain and leakage, only the influence of switched voltage is considered. If the switch control is based on the displacement induced by the external force, the $(2k-1)$th harmonic components of switched voltage on piezoelectric element is

$$V_{\mathrm{sw},(2k-1)}(t)=\hat{V}_{\mathrm{sw}}\frac{4}{(2k-1)\pi}\sin(2k-1)\omega_et=H\frac{\alpha_i\beta u_{iM}}{C_p}\frac{4}{(2k-1)\pi}\sin(2k-1)\omega_et. \tag{50}$$

Here it is assumed that $(2k-1)\omega_e$ is near the natural frequency of the jth mode. Based on vibration response for the ith mode (48), the response of the jth mode due to the force in Eq. (50) can be obtained and expressed in the following form:

$$u_{jM}=\frac{\alpha_j\cdot H\frac{\alpha_i\beta u_{iM}}{C_p}\frac{4}{(2k-1)\pi}/K_{Dj}}{\sqrt{\left(1-\left(\frac{(2k-1)\omega_e}{\omega_{nj}}\right)^2\right)^2+\left[2\left(\frac{(2k-1)\omega_e}{\omega_{nj}}\right)\zeta_j\right]^2}}=\frac{4}{(2k-1)\pi}\cdot\frac{\beta HK_{sij}}{\sqrt{\left(1-\left(\frac{(2k-1)\omega_e}{\omega_{nj}}\right)^2\right)^2+\left[2\left(\frac{(2k-1)\omega_e}{\omega_{nj}}\right)\zeta_j\right]^2}}u_{iM} \tag{51}$$

The above equation gives a ratio between the vibration amplitude of the mode to be control and that of the undesired vibration of the of jth mode, u_{jM}/u_{iM}. It indicates that the amplitude ratio depends on many factors. For simplicity, it is assumed that $\omega_e=\omega_{ni}$. In the worst case that $\omega_{nj}=(2k-1)\omega_{ni}$, the amplitude of the undesired vibration reaches maximum and the amplitude ratio is

$$\frac{u_{jM}}{u_{iM}}=\frac{4}{(2k-1)\pi}\cdot\frac{\beta HK_{sij}}{2\zeta_j}=\frac{4}{(2k-1)\pi}\cdot\frac{K_{sij}Q_{mj}}{K_{sii}Q_{mi}}\cdot\beta HK_{sii}Q_{mi}. \tag{52}$$

According to Eq. (46), it is important to increase the value of $\beta HK_{sii}Q_{mi}$ in order to improve the control performance. However, Eq. (52) indicates that the amplitude ratio is directly proportional to $\beta HK_{sii}Q_{mi}$. Hence, in a real vibration control system, it is important to decrease the value of $(K_{sij}Q_{mj})/(K_{sii}Q_{mi})$. Fortunately, the condition $\omega_{nj}=(2k-1)\omega_{ni}$ is rarely satisfied in a real engineering structure. On the other hand, the ratio u_{jM}/u_{iM} is also reduced as k increases. Undesirable excitation of high-order modes can also be alleviated by increasing the time constant of the switch circuit. It will be topic of future works.

4. Verification experiments and simulation

4.1. Experimental setup

Experimental validation of performance of unsymmetrical SSDV control was carried out using a cantilever beam shown in Fig. 4. The length, width and thickness of the beam with bonded piezoelectric actuators are 1200 mm, 76 mm and 1.5 mm, respectively. The natural frequencies of the first two modes are 0.98 Hz and 6.1 Hz, respectively. The beam is excited by an electromagnetic shaker at the clamped end. The damping ratios of the two modes are 1.79% and 0.81%.

Two MFC actuators, numbered 1 and 2, are bonded on one side of the beam and used to control the first two modes of the beam separately. The in-plane size of the MFCs is 103 mm by 64 mm and their thickness is 0.3 mm. The material properties of the beam and piezoelectric patches are shown in Tables 1 and 2. The MFC 1 was used to control the second mode and the MFC 2 was used to control the first mode. The displacement of the beam at a distance of 700 mm from its clamped end was measured by a laser displacement sensor and the signal was used for switch control in the shunt circuit. The schematic chart of the control system is shown in Fig. 5.

Experiments of both single-mode control and two-mode control were carried out. In two-mode control, the modal displacements of the beam were identified online using a state observer and used for switch control of the two MFC actuators. When an extremum was detected in the modal displacement signal, a trigger signal was generated to turn on the electronic switch in the shunt circuit so that the voltage on the piezoelectric patches was inverted. For the purpose of comparison, control experiments using both the symmetrical SSDV and unsymmetrical SSDV approaches were carried under the same excitation condition. To illustrate the advantage of unsymmetrical SSDV, the control performances of the symmetrical SSDV and unsymmetrical SSDV approaches were compared when the same maximum negative voltage was generated on the actuator.

4.2. Experimental results and discussion

4.2.1. Results of single mode control

Experiments of single-mode control were carried out first to validate the control performance of the unsymmetrical SSDV method. In the experiment of single-mode control, the beam was excited by a pure tone at one of the resonance frequencies. Both symmetrical and unsymmetrical switching of the actuator voltage were considered for comparison. Since the capacitance of the MFC actuator is very small, the actuator voltage is very sensitive to the leakage in the switch circuit when the switching frequency is low. In order to alleviate the influence of leakage, a capacitor of 1 μF is connected to the piezoelectric actuator in parallel to reduce the influence of the circuit leakage.

4.2.1.1. Symmetrical switching. First, the beam is excited at 0.98 Hz, the resonance frequency of the first mode. The dotted line in Fig. 6(a) shows the spectrum of displacement in the frequency range from 0 Hz to 10 Hz. The peak at this frequency is dominant, but there are also peaks at the high-order harmonics because of the nonlinearity of the system. The voltage on MFC 2 was switched using a symmetrical SSDV circuit with an output voltage source equal to 13 V. The voltages V_{Mp} , $-V_{Mn}$,

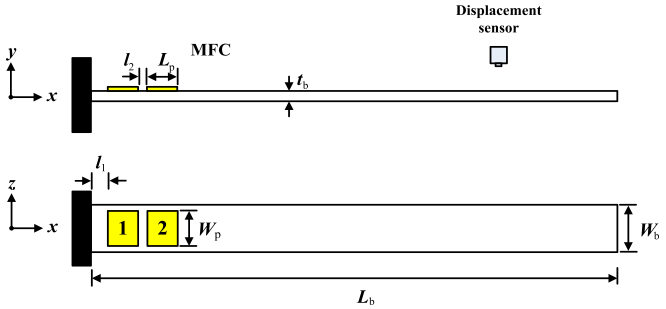

Fig. 4. Beam with two piezoelectric patches.

Table 1
Material properties of the cantilever beam.

	Beam
Elastic modulus	7.2×10^{10} [N/m^2]
Poisson ratio	0.34
Shear modulus	1.25×10^{10} [N/m^2]
Density	2700 [kg/m^3]

Table 2
Material properties of the MFCs.

	MFCs
Elastic modulus	59×10^9 [N/m^2]
Poisson ratio	0.345
Density	7400 [kg/m^3]
Piezoelectric constant d_{31}	-260×10^{-12} [m/V]
Free capacity C_{p0}	141×10^{-9} [F]

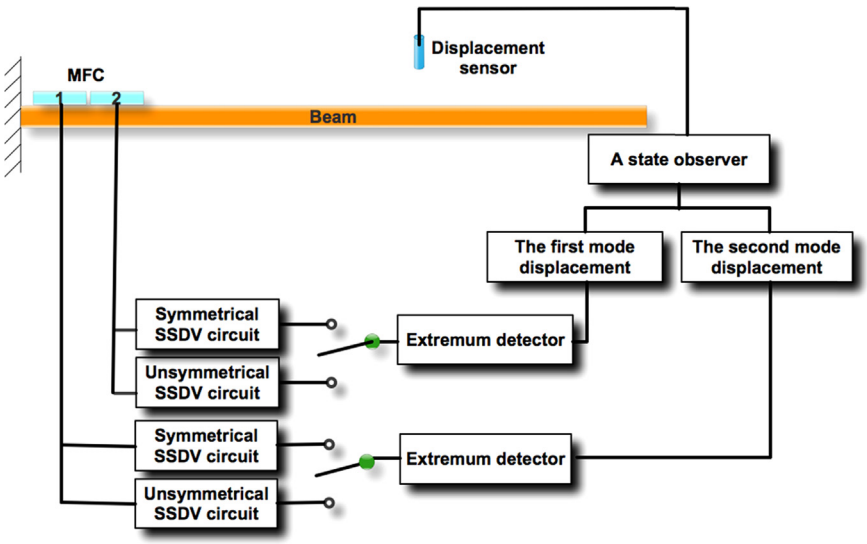

Fig. 5. The schematic of the control system.

$V^{\mathrm{p}}_{\mathrm{sw}}$, and $V^{\mathrm{n}}_{\mathrm{sw}}$, which are defined in Fig. 3, are 71.73 V, −68.96 V, 74.8 V, and −72.4 V, respectively. The slight difference between the value of maximum voltage and the absolute value of minimum voltage in symmetrical SSDV control is probably due to the difference in the electronic elements in different branches of the switch circuit.

The dominant peak at 0.98 Hz is reduced from 14.57 dB to 7.35 dB, as shown in Fig. 6(a). Fig. 6(b) shows the displacement variation in the time domain. The amplitude of displacement was reduced by 60% after control. However, the spectrum in Fig. 6(a) also shows that some peaks at the high-order harmonic frequencies have been amplified. This is because the switched voltage contains both the fundamental harmonic and high-order harmonic components. The high-order components were not considerably excited in this study because the frequencies of both the 5th and 7th harmonic are significantly different from the natural frequency of the 2nd mode, which is 6.1 Hz [26].

Fig. 7 shows the results of symmetrical SSDV control at the second resonance frequency of 6.1 Hz when the voltage of MFC 1 is switched with a voltage source of 13 V. The displacement amplitude of the second mode was reduced by 5.91 dB in symmetrical SSDV. The voltage drop due to circuit leakage in Fig. 7(c) is apparently smaller in comparison with Fig. 6(c) due to higher switching frequency. The voltages V_{Mp}, $-V_{Mn}$, $V^{\mathrm{p}}_{\mathrm{sw}}$, and $V^{\mathrm{n}}_{\mathrm{sw}}$ are 94.67 V, −93.5 V, 95.42 V, and −94.23 V, respectively.

4.2.1.2. Unsymmetrical switching. Experiments of unsymmetrical SSDV control of the cantilever beam were carried out under the same excitation condition. A bypass capacitance of 2 μF was used to generate an unsymmetrical voltage on actuator. Fig. 8 shows the results of unsymmetrical SSDV control at the first resonance frequency when the voltage of MFC 2 is switched with a voltage source of 14 V. The voltages V_{Mp}, $-V_{Mn}$, $V^{\mathrm{p}}_{\mathrm{sw}}$, and $V^{\mathrm{n}}_{\mathrm{sw}}$ are 90.2 V, −52.6 V, 93.8 V, and −53.4 V, respectively. The voltage source was set to 14 V to keep the magnitude of switched voltage $\hat{V}_{\mathrm{sw}}$ at 73.6 V, the same as that in symmetrical SSDV control. The displacement amplitude of the first mode was reduced by 5.91 dB in unsymmetrical SSDV, which is almost the same with symmetrical SSDV control. This result confirms the theoretical conclusion that the control performance depends on $\hat{V}_{\mathrm{sw}}$, as shown in Eq. (51).

A large value of $\hat{V}_{\mathrm{sw}}$ in unsymmetrical SSDV was achieved with a voltage source of 19.7 V. The control results are shown in Fig. 9, which exhibit considerably better control performance. The dominant peak at 0.98 Hz is reduced from 14.57 dB to −5.97 dB. A 20.6 dB reduction was achieved. The voltages V_{Mp}, $-V_{Mn}$, $V^{\mathrm{p}}_{\mathrm{sw}}$, and $V^{\mathrm{n}}_{\mathrm{sw}}$ are 120 V, −70.3 V, 124.7 V, and −71.5 V, respectively. It indicates that the magnitude of switch voltage $\hat{V}_{\mathrm{sw}}$ was effectively raised from 73.6 V to 98.1 V, almost without changing the maximum negative voltage. It also means that the capability of the piezoelectric can be effectively utilized based on unsymmetrical switching. The control performances of the single mode control for the first mode using symmetrical SSDV and unsymmetrical SSDV are summarized in Table 3.

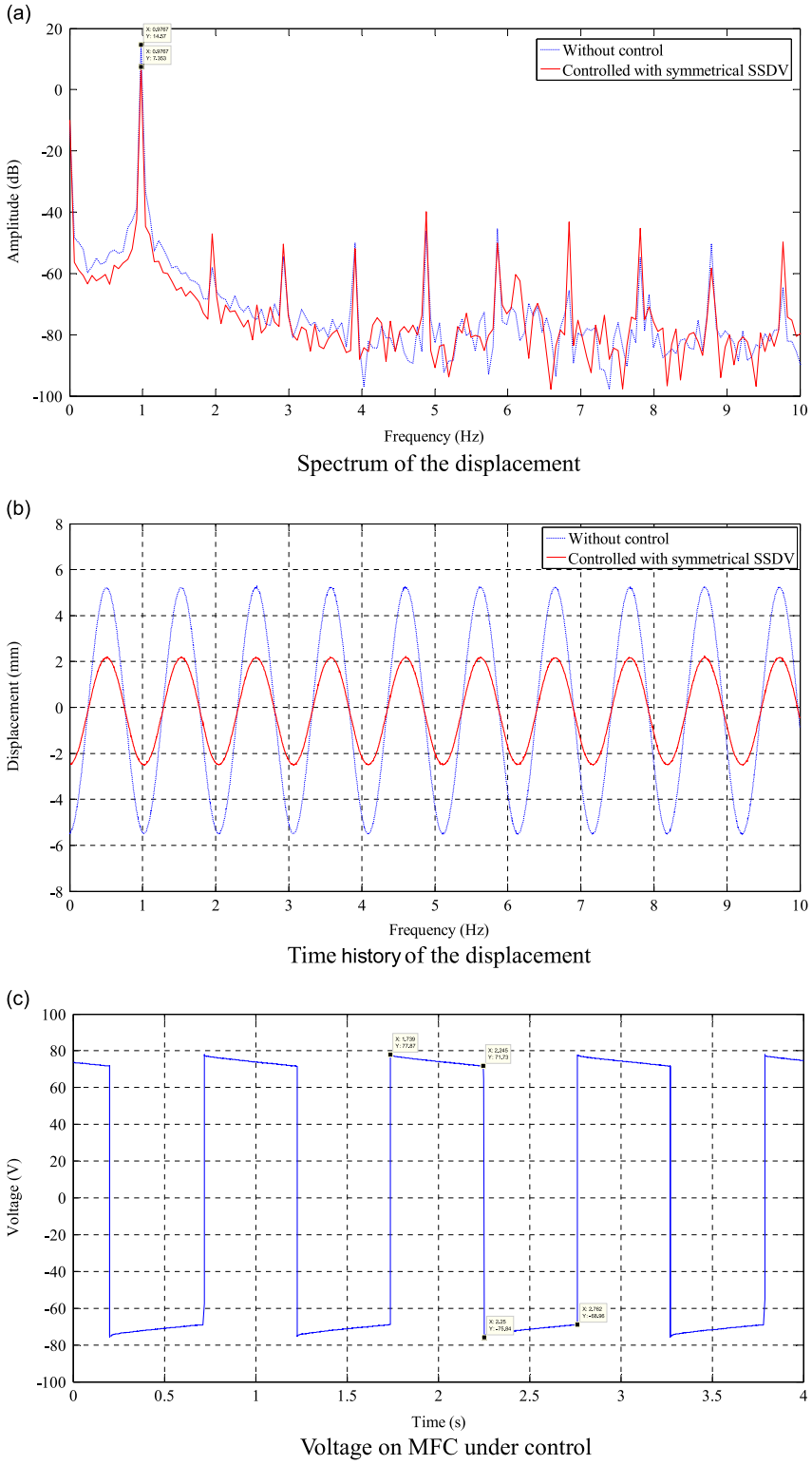

Fig. 6. The control performance of first mode using symmetrical SSDV method. (a) Spectrum of the displacement. (b) Time history of the displacement. (c) Voltage on MFC under control.

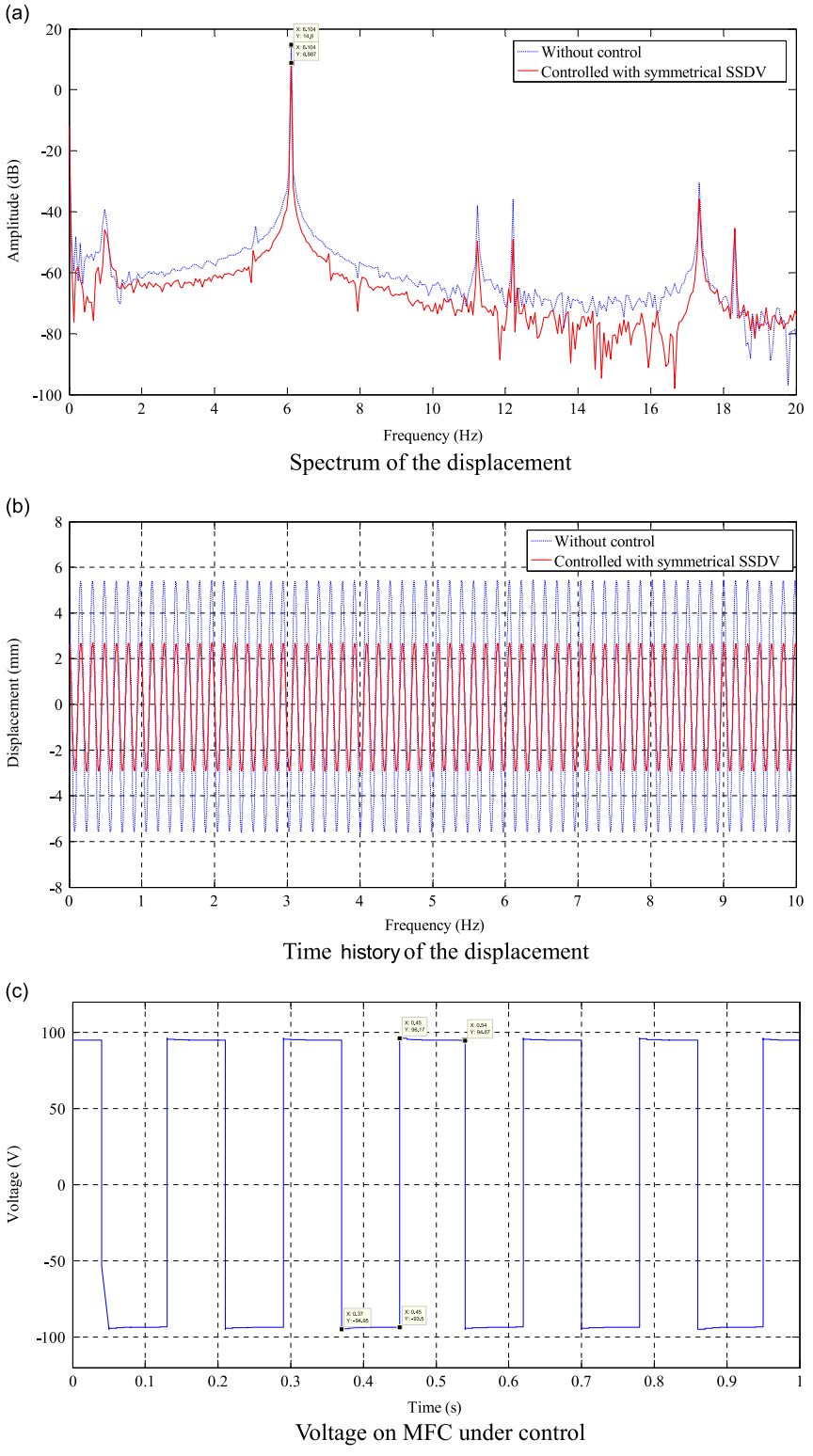

Fig. 7. The control performance of second mode using symmetrical SSDV method. (a) Spectrum of the displacement. (b) Time history of the displacement. (c) Voltage on MFC under control.

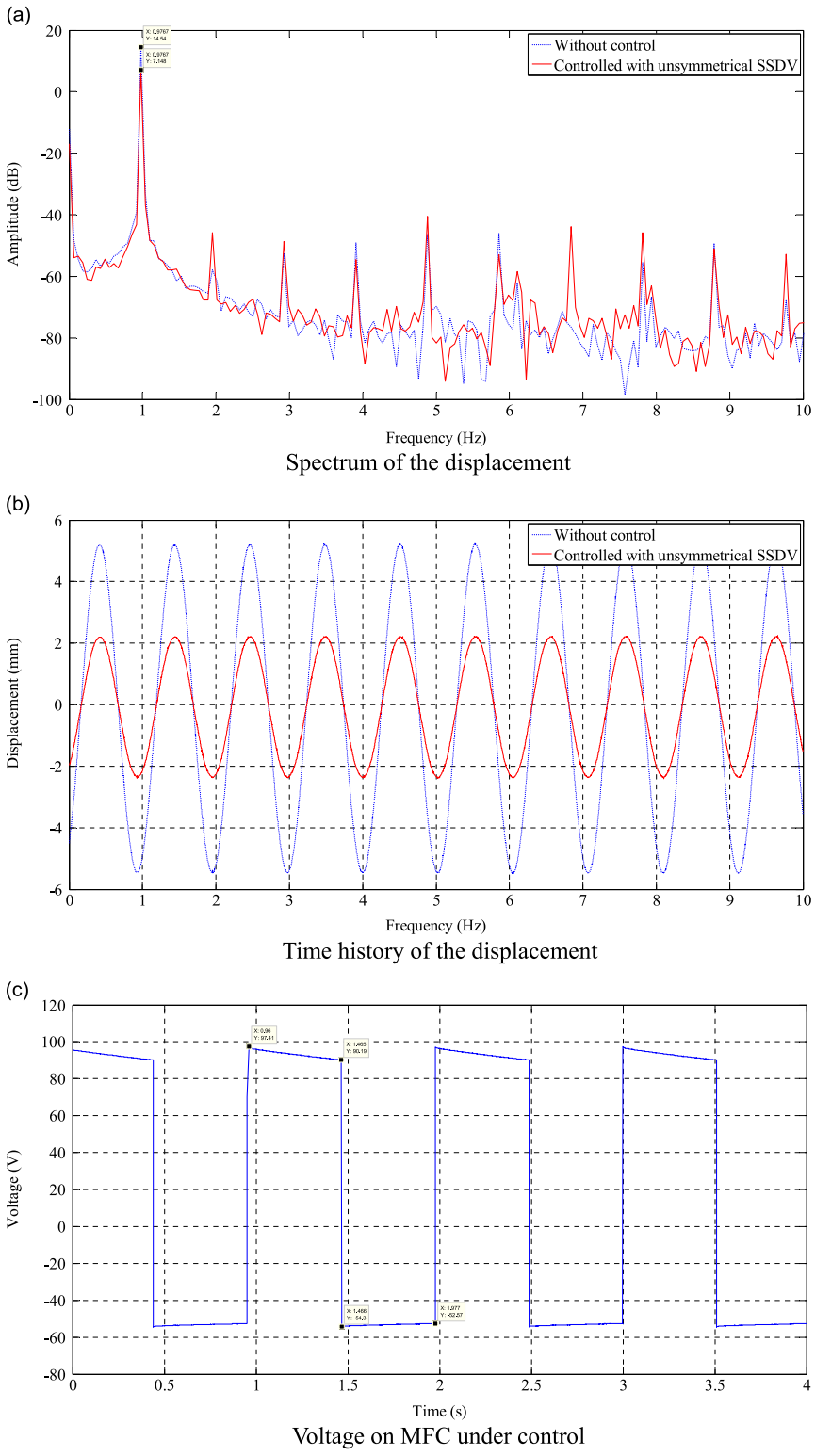

Fig. 8. The control performance of first mode using unsymmetrical SSDV method (keep the same $\hat{V}_{sw}$ as in symmetrical SSDV). (a) Spectrum of the displacement. (b) Time history of the displacement. (c) Voltage on MFC under control.

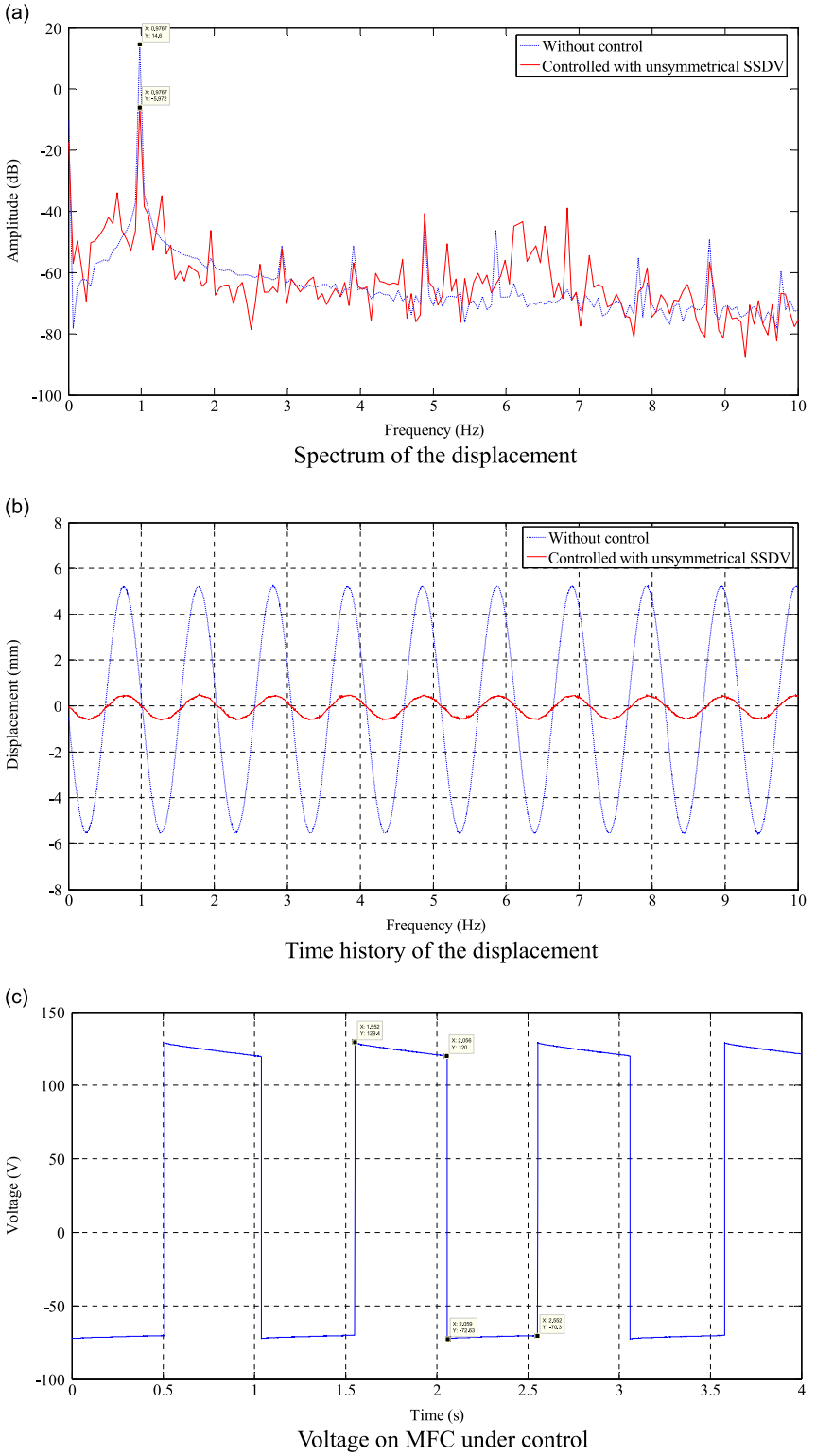

Fig. 9. The control performance of first mode using unsymmetrical SSDV method (keep larger $\hat{V}_{sw}$ than in symmetrical SSDV). (a) Spectrum of the displacement. (b) Time history of the displacement. (c) Voltage on MFC under control.

Table 3
Comparison of the control performances of the first mode control.

First mode control	V_{cc} (V)	V_{Mp} (V)	V_{mp} (V)	V_{sw}^{p} (V)	$-V_{Mn}$ (V)	$-V_{mn}$ (V)	$-V_{sw}^{n}$ (V)	$\hat{V}_{sw}$ (V)	Control performance (dB)
Symmetrical SSDV	13	71.7	77.9	74.8	−69.0	−75.8	−72.4	73.6	−7.22
Unsymmetrical SSDV	13.8	90.2	97.4	93.8	−52.6	−54.3	−53.4	73.6	−7.39
Unsymmetrical SSDV	19.7	120	129.4	124.7	−70.3	−72.6	−71.5	98.1	−20.57

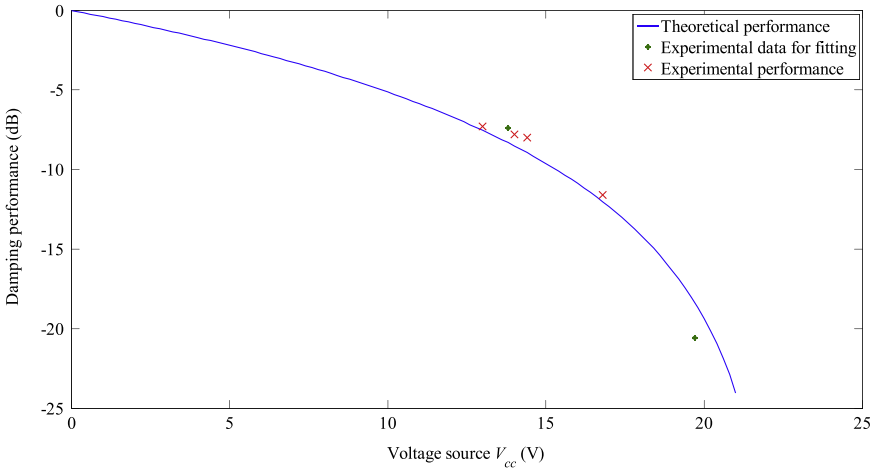

Fig. 10. Comparison of experimental and theoretical results of the control performance as a function of voltage source.

The control performance of adaptive SSDV, in which the output of voltage source is proportional to displacement amplitude, is given by Eq. (53). It indicates that the displacement amplitude approaches zero as the ratio β approaches infinity. In this study, the output of the voltage source is directly given for the purpose of comparison reasons. In that case, the attenuation can be expressed by

$$A_{\mathrm{ASSDV}} = 20\log\left(\frac{u_{iM}}{\overline{u}_{iM}}\right) = -20\log\left|1-\frac{4}{\pi}\cdot\frac{\alpha_i H}{F_e}V_{\mathrm{cc}}\right|. \tag{53}$$

This expression means that there is an optimal voltage source, V_{cc}^{opt}, that completely cancels the vibration generated by the excitation force.

The expression of H in Eq. (53) is very complicated, as shown in Eq. (46). It may also vary with V_{cc} because the properties of leakage change with the switched voltage. For convenience, H is assumed to be constant and the value of $\alpha_i H/F_e$ in Eq. (53) is directly calculated from the experimental results in Table 3 using the least square method. The result is 0.0351. The theoretical curve of Eq. (53) is plotted in Fig. 11. Control experiments were also carried at $V_{cc}=13$, 14, 14.4, 16.8 for validation. All the experimental results are also plotted in Fig. 10, with the results used for estimation of $\alpha_i H/F_e$ marked by "*", and the results for validation marked by "$\times$". Although it has been assumed that H in Eq. (53) is constant, the experimental results agree well with the theoretical results.

An experiment was also conducted at the second mode of 6.1 Hz. Two cases, one with the same $\hat{V}_{\mathrm{sw}}$ as that in symmetrical SSDV and the other with larger $\hat{V}_{\mathrm{sw}}$ than that in symmetrical SSDV, were considered. The voltage source was set to 14.6 V to generate a switched voltage $\hat{V}_{\mathrm{sw}}$ of 94.7 V, the same as that in symmetrical SSDV control. The dominant peak of the second mode was reduced by 5.83 dB in unsymmetrical SSDV, which is almost the same as that in symmetrical SSDV control, as shown in Fig. 11(a). This experimental result validates the theoretical conclusion that the control performance is determined by the magnitude of switched voltage, $\hat{V}_{\mathrm{sw}}$, regardless of symmetrical or unsymmetrical switching. Fig. 11(b) shows the corresponding displacement in the time domain, showing a 50% reduction of the displacement as a result of control.

By increasing the output of the voltage source, better control performance can be achieved. When $V_{cc}=20.7$ V, the magnitude of switch voltage, $\hat{V}_{\mathrm{sw}}$, was 126.2 V, and the amplitude of displacement was significantly reduced after control as shown in Fig. 12. A reduction of 17 dB was achieved at the resonance peak of 6.1 Hz. Compared with symmetrical SSDV, the negative switched voltage $\hat{V}_{\mathrm{sw}}^{\mathrm{n}}$ is almost the same, but the value of $\hat{V}_{\mathrm{sw}}$ was increased from 94.8 V in symmetrical SSDV to 126.2 V in unsymmetrical SSDV and the control performance was significantly improved, too. The result also indicates that unsymmetrical SSDV can make better utilization of the actuator capacity. The performances of the single mode control for the second mode using symmetrical SSDV and unsymmetrical SSDV are summarized in Table 4.

4.2.2. Results of two-mode control

The two-mode control scheme attempts to control both structural modes simultaneously. In the experiments, the beam was excited simultaneously by two harmonic frequencies at 0.98 Hz and 6.1 Hz. The spectrum of the displacement is shown by the dotted line in Fig. 13(a). The peaks at the two frequencies of excitation are dominant, but there are also small peaks at other frequencies. The two MFCs were switched by two independent circuits for controlling the first and the second mode separately, as shown in Fig. 5. The modal displacements of the two modes were identified by a state observer and used in the action control of the two switches [27]. The outputs of the voltage sources in the two switches were set to 20 V and 18.5 V, respectively. The spectrum of the controlled displacement is shown in Fig. 13(a), which shows that the peak at 0.98 Hz is reduced by 14.56 dB, whilst the one at 6.1 Hz by 14.92 dB. Fig. 13(b) shows the corresponding displacement

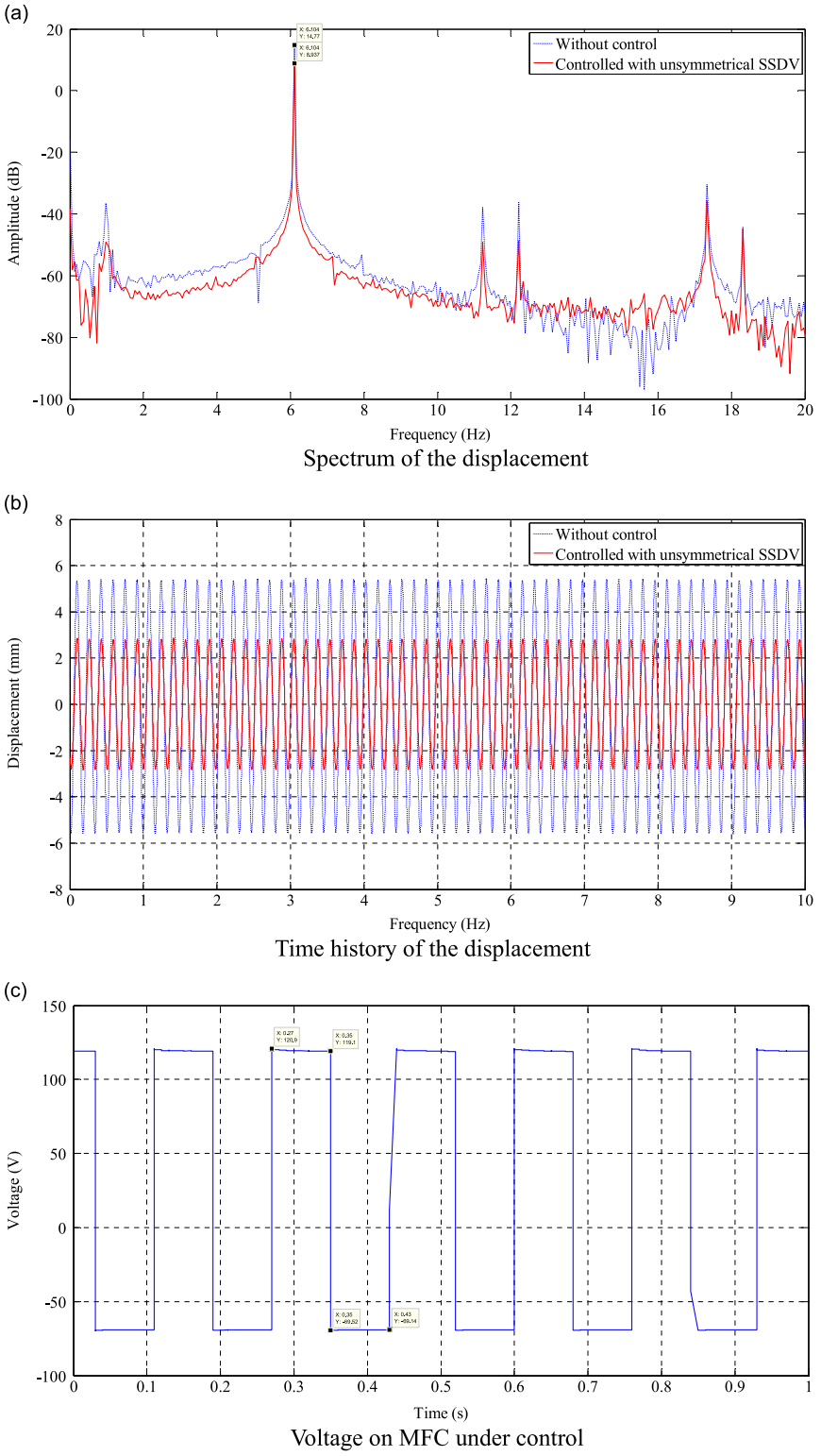

Fig. 11. The control performance of second mode using unsymmetrical SSDV method (keep the same $\hat{V}_{sw}$ as in symmetrical SSDV). (a) Spectrum of the displacement. (b) Time history of the displacement. (c) Voltage on MFC under control.

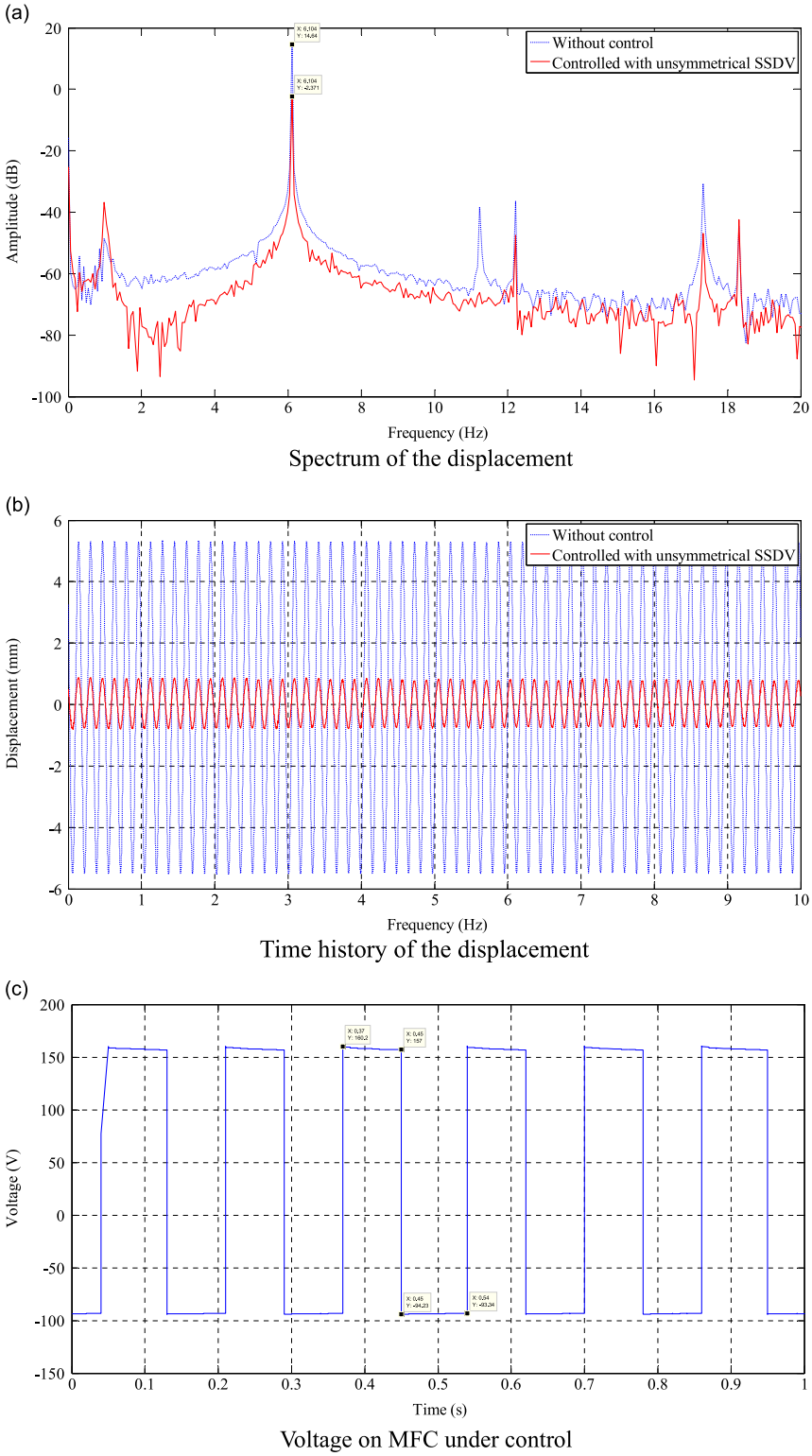

Fig. 12. The control performance of second mode using unsymmetrical SSDV method (keep larger $\hat{V}_{sw}$ than in symmetrical SSDV). (a) Spectrum of the displacement. (b) Time history of the displacement. (c) Voltage on MFC under control.

Table 4
Comparison of the control performances of the second mode control.

Second mode control	V_{cc} (V)	V_{Mp} (V)	V_{mp} (V)	V_{sw}^{p} (V)	$-V_{Mn}$ (V)	$-V_{mn}$ (V)	$-V_{sw}^{n}$ (V)	$\hat{V}_{sw}$ (V)	Control performance (dB)
Symmetrical SSDV	13	94.7	96.2	95.4	−93.5	−95.0	−94.2	94.8	−5.91
Unsymmetrical SSDV	14.6	119.1	120.9	120	−69.1	−69.5	−69.3	94.7	−5.83
Unsymmetrical SSDV	20.7	157	160.2	158.6	−93.3	−94.2	−93.8	126.2	−17.01

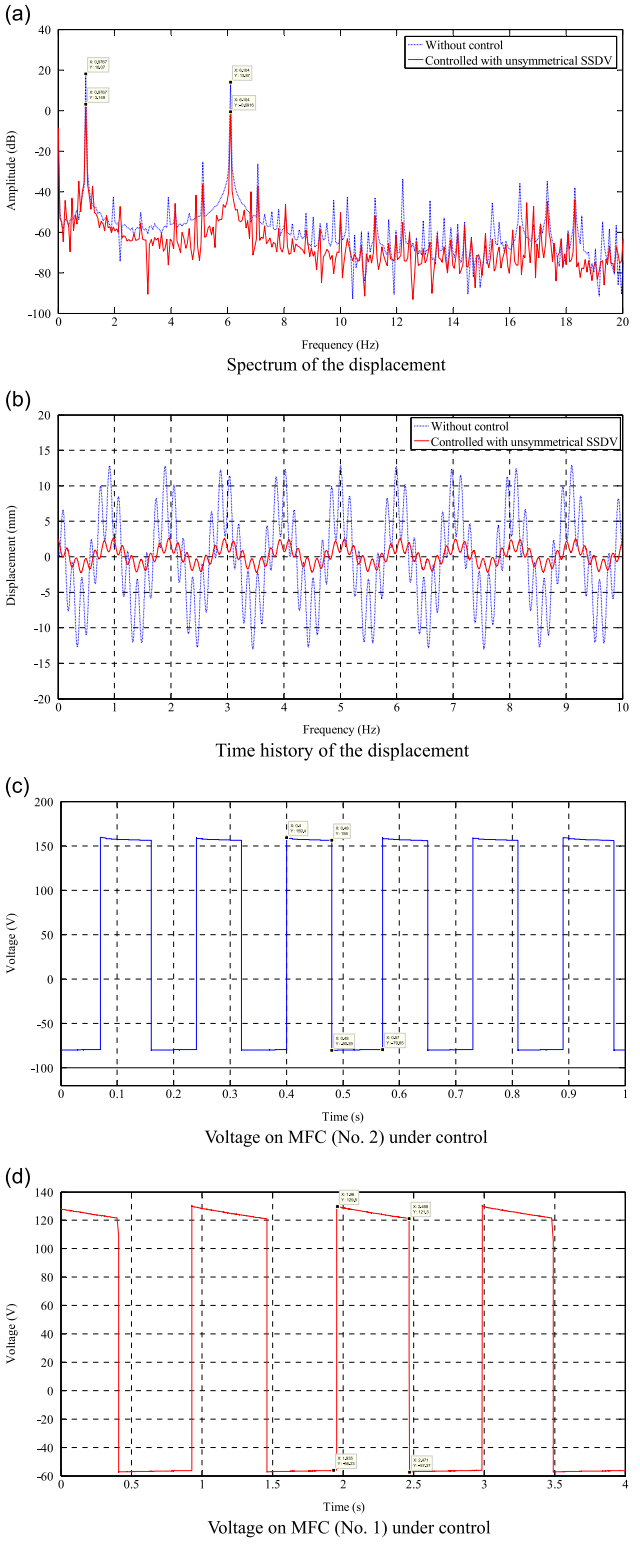

Fig. 13. The control performance of two-mode using unsymmetrical SSDV method. (a) Spectrum of the displacement. (b) Time history of the displacement. (c) Voltage on MFC (No. 2) under control. (d) Voltage on MFC (No. 1) under control.

Table 5
The control performances of the two-mode control.

	V_{cc} (V)	V_{Mp} (V)	V_{mp} (V)	V_{sw}^{p} (V)	$-V_{Mn}$ (V)	$-V_{mn}$ (V)	$-V_{sw}^{n}$ (V)	$\hat{V}_{sw}$ (V)	Control performance (dB)
First mode	20	156	159.4	157.7	−79.7	−80.3	−80	118.9	−14.56
Second mode	18.5	121.3	129.8	125.6	−57.4	−56.2	−56.8	91.2	−14.92

variation in the time domain. The amplitude of the displacement is reduced significantly. The control performances of the two-mode control using different methods are summarized in Table 5.

5. Conclusion

An unsymmetrical SSD switch circuit has been designed in the previous paper to increase the effective voltage range on the PZT actuator to improve the control performance. In this study, analysis and experimental validation of control performance of a synchronized switch damping system based on the unsymmetrical switch circuit was carried out. Based on its periodicity in steady-state control, the harmonic components of the actuator voltage was derived using Fourier series expansion. The displacement response of the system was derived under combined actions of the excitation and switched voltage. In the analysis of system response, the influence of leakage on the switched voltage was taken into consideration, but the transient process of leakage was neglected. The damping effect of the unsymmetrical SSDV with different voltage source was derived. An experimental setup of a beam was built to validate the control performance. The results showed that the control performance mainly depends on the voltage range on the PZT, and the same control performance can be achieved in both unsymmetrical SSD, and symmetrical SSD when the same voltage range on the PZT is applied. Due to the intrinsic unsymmetrical properties of piezoelectric actuators, a higher effective voltage range can be generated in unsymmetrical SSDV than in symmetrical SSDV and better control performance can be achieved at the same negative actuator voltage. The theoretical and experimental results verify the advantages of the unsymmetrical SSDV and the fact that it makes better utilization of the actuator capability.

Acknowledgment

This research is supported by the National Natural Science Foundation of China under Grant 51375228, Aeronautical Science Fund under Grant 20131552025, Natural Science Foundation of Jiangsu Province, China under Grant BK20130791, China Postdoctoral Science Special Foundation under Grant 2014T70514, the Fundamental Research Funds for the Central Universities under Grant NE2015001, and PAPD.

Appendix A

The Fourier coefficients of the three components in the actuator voltage are derived below.

Expansion of strain-induced voltage

The Fourier expansion of $V_{st}(t)$ can be expressed in the following form:

$$V_{st}(t)=F\{V_{st}(t)\}=\frac{a_0^{st}}{2}+\sum_{k=1}^{\infty}\left(a_k^{st}\cos k\frac{\omega_{sw}}{2}t+b_k^{st}\sin k\frac{\omega_{sw}}{2}t\right). \tag{A1}$$

According to the theory of Fourier series, the coefficients in the above expression can be calculated using the voltage in Eq. (11). The coefficients are as follows:

$$\begin{cases} a_0^{st}=\int_{-T_{sw}}^{T_{sw}}V_{st}(t)dt=0 \\ a_1^{st}=\int_{-T_{sw}}^{T_{sw}}V_{st}(t)\cos\frac{\omega_{sw}}{2}tdt=-\frac{\alpha u_M}{2}\left(\frac{1}{C_p+C_b}+\frac{1}{C_p}\right) \\ a_k^{st}=\int_{-\tau_{sw}}^{\tau_{sw}}V_{st}(t)\cos k\frac{\omega_{sw}}{2}tdt=0,\quad (k>1) \\ b_1^{st}=\int_{-\tau_{sw}}^{\tau_{sw}}V_{st}(t)\sin\frac{\omega_{sw}}{2}tdt=0 \\ b_k^{st}=\int_{-\tau_{sw}}^{\tau_{sw}}V_{st}(t)\sin k\frac{\omega_{sw}}{2}tdt=-\frac{\alpha u_M}{\pi}\frac{C_b}{C_p(C_p+C_b)}\frac{k}{k^2-1}\left[1+(-1)^k\right],(k>1) \end{cases} \tag{A2}$$

Since $a_1^{st} \neq 0$, the strain-induced voltage has influence on the fundamental harmonic. However, because a_1^{st} is the coefficient of the cosine term, the voltage only generates an additional stiffness, not damping effect. The voltage will also generate high even-order harmonic vibration because $b_k^{st} \neq 0$ when k is even.

Expansion of switched voltage

The Fourier expansion of switched voltage $V_{sw}(t)$ is expressed in the following form:

$$V_{sw}(t) = \mathcal{F}\{V_{sw}(t)\} = \frac{a_0^{sw}}{2} + \sum_{k=1}^{\infty}\left(a_k^{sw}\ \cos\ k\frac{\omega_{sw}}{2}t + b_k^{sw}\ \sin\ k\frac{\omega_{sw}}{2}t\right). \tag{A3}$$

Based on the switched voltage in Eq. (16) and the formulas of Fourier expansion for rectangular waveform, the switched voltage can be expressed in the following form:

$$V_{sw}(t) = \overline{V}_{sw} + \hat{V}_{sw}S_{\tau_{sw}}(t) = \overline{V}_{sw} + \hat{V}_{sw}\sum_{k=1}^{\infty}\frac{4}{(2k-1)\pi}\sin\frac{2k-1}{2}\omega_{sw}t \tag{A4}$$

The above expression indicates

$$\begin{cases} \frac{a_0^{sw}}{2} = \overline{V}_{sw} \\ a_k^{sw} = 0, \quad (k = 1, 2, \cdots) \\ b_k^{sw} = \begin{cases} \frac{4}{(2i-1)\pi}\hat{V}_{sw} & (k = 2i-1, i = 1, 2, \cdots) \\ 0 & (k = 2i, i = 1, 2, \cdots) \end{cases} \end{cases} \tag{A5}$$

The results indicate that the switched voltage consists of a DC component and the odd-order harmonics. The fundamental harmonic will generate a control force to suppress the vibration excited by external force, but the other components will excite vibration at the higher odd-order harmonic frequencies.

Expansion of leakage voltage

The Fourier expansion of transient leakage voltage $V_L(t)$ is expressed in the following form:

$$V_L(t) = F\{V_L(t)\} = \frac{a_0^L}{2} + \sum_{k=1}^{\infty}\left(a_k^L\ \cos\ k\frac{\omega_{sw}}{2}t + b_k^L\ \sin\ k\frac{\omega_{sw}}{2}t\right) \tag{A6}$$

Using the formula of Fourier series, the coefficients in Eq. (A6) can be calculated as follows.

$$\begin{cases} a_0^L = \frac{1}{T_{sw}}\left[\int_{-T_{sw}}^{0} V_L^n(t)dt + \int_0^{T_{sw}} V_L^p(t)dt\right] = \frac{V_{Ln}}{\pi}\left(\frac{\overline{b}'\pi^2}{\omega} + \overline{c}'\pi + \overline{f}'\pi - \frac{\overline{c}'\omega}{2d'} - \frac{\overline{f}'\omega}{2g'}\right) - \frac{V_{Lp}}{\pi}\left(\frac{\overline{b}\pi^2}{\omega} + \overline{c}\pi + \overline{f}\pi - \frac{\overline{c}\omega}{2d} - \frac{\overline{f}\omega}{2g}\right) \\ a_k^L = \frac{1}{T_{sw}}\left[\int_{-T_{sw}}^{0} V_L^n(t)\ \cos\ k\frac{\omega_{sw}}{2}t\ dt + \int_0^{T_{sw}} V_L^p(t)\cos\ k\frac{\omega_{sw}}{2}\right] = \frac{V_{Lp}}{k\pi}\left(\frac{2dk\omega\overline{c}}{4d^2+k^2\omega^2} + \frac{2gk\omega\overline{f}}{4g^2+k^2\omega^2}\right) - (-1)^k\frac{V_{Ln}}{k\pi}\left(\frac{2d'k\omega\overline{c}'}{4d'^2+k^2\omega^2} + \frac{2g'k\omega\overline{f}'}{4g'^2+k^2\omega^2}\right) \\ b_k^L = \frac{1}{T_{sw}}\left[\int_{-T_{sw}}^{0} V_L^n\ \sin\ k\frac{\omega_{sw}}{2}t\ dt + \int_0^{T_{sw}} V_L^p\ \sin\ k\frac{\omega_{sw}}{2}t\ dt\right] = \frac{V_{Lp}}{k\pi}\left[\left(1-(-1)^k\right)\left(\frac{1}{2} - \overline{c} - \overline{f}\right) + (-1)^k\frac{2\overline{b}\pi}{\omega} + \frac{k^2\omega^2\overline{c}}{4d^2+k^2\omega^2} + \frac{k^2\omega^2\overline{f}}{4g^2+k^2\omega^2}\right] \\ \qquad -(-1)^k\frac{V_{Ln}}{k\pi}\left[\left(1-(-1)^k\right)\left(\frac{1}{2} - \overline{c}' - \overline{f}'\right) + (-1)^k\frac{2\overline{b}'\pi}{\omega} + \frac{k^2\omega^2\overline{c}'}{4d'^2+k^2\omega^2} + \frac{k^2\omega^2\overline{f}'}{4g'^2+k^2\omega^2}\right] \end{cases} \tag{A7}$$

In the simplification of the above expression, it has been assumed that $dT_{sw}, gT_{sw}, d'T_{sw}, g'T_{sw}$ are larger enough and $e^{-dT_{sw}} = e^{-gT_{sw}} = e^{-d'T_{sw}} = e^{-g'T_{sw}} = 0$. In the experimental conditions of this study, these assumptions are satisfied.

Using the coefficients $\overline{b}, \overline{b}', \overline{c}, \overline{c}', \overline{f}, \overline{f}'$ obtained in the former study [22], it can easily be confirmed that coefficients of V_{Lp} and V_{Ln} in Eq. (A7) are much smaller than one. One the other hand, V_{Lp} and V_{Ln} are much smaller than $\hat{V}_{sw}$. Hence, the influence of transient variation due to leakage can be neglected.

References

[1] C. Richard, D. Guyomar, D. Audigier, G. Ching, Semi-passive damping using continuous switching of a piezoelectric device, *Proceedings of SPIE Conference on Passive Damping and Isolation* (*Newport Beach*), Vol. 3672, SPIE Optical Engineering Press Bellingham, WA, 1999, pp. 104–111.

[2] C. Richard, D. Guyomar, D. Audigier, H. Bassaler, Enhanced semi passive damping using continuous switching of a piezoelectric device on an inductor, *Proceedings of SPIE International Symposium on Smart Structures and Materials*: *Damping and Isolation*, Vol. 3989, 2000, pp. 288–299.

[3] K. Makihara, J. Onoda, K. Minesugi, Using tuned electrical resonance to enhance bang-bang vibration control, *AIAA Journal* 45 (2007) 497–504.

[4] Y. Wang, A. Erturk, D. Inman, Comparison of control laws for vibration suppressions based on energy consumption, *Journal of Intelligent Material Systems and Structures* 22 (8) (2010) 795–809.
[5] J.R. Liang, H.S.H. Chung, W.H. Liao, Dielectric loss against piezoelectric power harvesting, *Smart Materials and Structures* 23 (9) (2014) 092001.
[6] J.R. Liang, W.H. Liao, Impedance modeling and analysis for piezoelectric energy harvesting systems, *IEEE/ASME Transactions on Mechatronics* 17 (6) (2012) 1145–1157.
[7] D. Guyomar, C. Richard, L. Petit, Non-linear system for vibration damping, *Proceedings of the 142th Meeting of Acoustical Society of America*, Fort Lauderdale, USA, 2001.
[8] K. Makihara, J. Onoda, K. Minesugi, A self-sensing method for switching vibration suppression with a piezoelectric actuator, *Smart Materials and Structures* 16 (2007) 455–461.
[9] E. Lefeuvre, A. Badel, L. Petit, C. Richard, D. Guyomar, Semi-passive piezoelectric structural damping by synchronized switching on voltage sources, *Journal of Intelligent Material Systems and Structures* 17 (2006) 653–660.
[10] A. Badel, G. Sebald, D. Guyomar, M. Lallart, E. Lefeuvre, C. Richard, J.H. Qiu, Piezoelectric vibration control by synchronized switching on adaptive voltage sources: towards wideband semi-active damping, *Journal of the Acoustical Society America* 119 (2006) 2815–2825.
[11] H.L. Ji, J.H. Qiu, A. Badel, K.J. Zhu, Semi-active vibration control of a composite beam using an adaptive SSDV approach, *Journal of Intelligent Material Systems and Structures* 20 (2009) 401–412.
[12] H.L. Ji, J.H. Qiu, A. Badel, Y.S. Chen, K.J. Zhu, Semi-active vibration control of a composite beam by adaptive synchronized switching on voltage sources based on LMS algorithm, *Journal of Intelligent Material Systems and Structures* 20 (2009) 939–947.
[13] A. Khodayari, A. Ahmadi, S. Mohammadi, On physical realization of the wireless semi active real time vibration control based on signal statistical behavior, *Sensors and Actuators A: Physical* 167 (2011) 102–109.
[14] Bilal Mokrani, Gonçalo Rodrigues, Burda Ioan, Renaud Bastaits, Andre Preumont, Synchronized switch damping on inductor and negative capacitance, *Journal of Intelligent Material Systems and Structures* 23 (18) (2012) 2065–2075.
[15] Hongli Ji, Jinhao Qiu, Jun Cheng, Daniel Inman, Application of a negative capacitance circuit in synchronized switch damping techniques for vibration suppression, *Journal of Vibration and Acoustics* 133 (2011) 041015.
[16] H. Ji, J. Qiu, D. Guyomar, Influences of switching phase and frequency of voltage on piezoelectric actuator upon vibration damping effect, *Smart Materials and Structures* 20 (16) (2010) 015008.
[17] D. Guyomar, C. Richard, S. Mohammadi, Semi-passive random vibration control based on statistics, *Journal of Sound and Vibration* 307 (2007) 818–833.
[18] H.L. Ji, J.H. Qiu, K.J. Zhu, A. Badel, Two-mode vibration control using nonlinear synchronized switching damping based on the maximization of converted energy, *Journal of Sound and Vibration* 329 (2010) 2751–2767.
[19] A.ïda Chérif, Claude Richard, Daniel Guyomar, Saâd Belkhiat, Mounir Meddad, Simulation of multimodal vibration damping of a plate structure using a modal SSDI-Max technique, *Journal of Intelligent Material Systems and Structures* 23 (6) (2012) 675–689.
[20] S. Harari, C. Richard, L. Gaudiller, New semi-active multi-modal vibration control using piezoceramic components, *Journal of Intelligent Material Systems and Structures* 20 (2009) 1603–1613.
[21] K. Li, J.Y. Gauthier, D. Guyomar, Structural vibration control by synchronized switch damping energy transfer, *Journal of Sound and Vibration* 330 (2011) 49–60.
[22] H.L. Ji, J.H. Qiu, Hong Nie, Li Cheng, Semi-active vibration control based on unsymmetrical synchronized switching damping, *Journal of Intelligent Material Systems and Structures* (2016) 1–15, http://dx.doi.org/10.1177/1045389X15585898.
[23] A. Badel, M. Lagache, D. Guyomar, E. Lefeuvre, C. Richard, Finite element and simple lumped modelling for flexural nonlinear semi-passive damping, *Journal of Intelligent Material Systems and Structures* 18 (2007) 727–742.
[24] M. Lallart, E. Lefeuvre, C. Richard, D. Guyomar, Self-powered circuit for broadband, multimodal piezoelectric vibration control, *Sensors and Actuators A: Physical* 143 (2) (2008) 377–382.
[25] A. Erturk, D.J. Inman, On mechanical modeling of cantilevered piezoelectric vibration energy harvesters, *Journal of Intelligent Material Systems and Structures* 19 (2008) 1311–1325.
[26] Hongli Ji, Li Cheng, Jinhao Qiu, Hong Nie, Semi-active noise suppression based on SSD technique using piezoelectric elements, *Proceedings of the 43rd International Congress on Noise Control Engineering*, Melbourne, Australia, 2014, pp. 16–19.
[27] Hongli Ji, Jinhao Qiu, Hong Nie, Li Cheng, Semi-active vibration control of an aircraft panel using synchronized switch damping method, *International Journal of Applied Electromagnetics and Mechanics* 46 (2014) 879–893.